sciendo

Polish Journal of Chemical Technology, 26, 4, 1—7, 10.2478/pjct-2024-0033

Green preparation of argentum tungstate and characterization as nanorod with catalytic evaluation for synthesizing tetracyclic xanthenes and validation as anti-TB

Abdulrahman A. Almehizia[1], Mohamed A. Al-Omar[1], Ahmed M. Naglah[1], Hazem A. Ghabbour[2, 3], Ashraf S. Hassan[4*], Tamer K. Khatab[4]

[1]Department of Pharmaceutical Chemistry, College of Pharmacy, King Saud University, P.O. Box 2457, Riyadh 11451, Saudi Arabia
[2]School of health and biomedical sciences, RMIT University, Melbourne 3083, Australia
[3]Department of Medicinal Chemistry, Faculty of Pharmacy, University of Mansoura, Mansoura 35516, Egypt
[4]Organometallic and Organometalloid Chemistry Department, National Research Centre, Dokki 12622, Cairo, Egypt
[*]*Corresponding author:* e-mail: ashraf_salmoon@yahoo.com

The work presented a facile, one-step procedure as a green assembly process for preparing silver tungstate nanorod by hydrothermal technique via a chemical reaction between silver nitrate and sodium tungstate. The synthesized precipitate was characterized using X-ray diffraction (XRD) transmission electronic microscope (TEM) and scanning electron microscopy (SEM) to ensure the formation of crystallization and single-phase material. The prepared nanorods undergo a catalytic evaluation to synthesize tetrahydrobenzo[a] xanthene-11-one derivatives by a one-pot reaction of β-naphthol, dimedone, and aromatic aldehyde with a catalytic amount of silver tungstate under the solvent-free condition at 60–70 °C. ArgC is one of the L-arginine biosynthetic pathways of mycobacterium tuberculosis. The molecular docking explains that all the synthesized compounds presented high ligand ability for the targeted enzyme compared with xanthene-9-carboxylic acid as a reference.

Keywords: β-Naphthol, dimedone, silver, xanthene, tuberculosis.

INTRODUCTION

Hydrothermal and solvothermal syntheses are important branches of inorganic synthesis. Hydrothermal and solvothermal techniques are used to synthesize and grow conventional and advanced materials[1, 2]. Silver tungstate (Ag_2WO_4) is a photosensitive semiconductor that could act as a catalyst beneath mild irradiation. It has a bandgap of around 3.1-3.2 eV, allowing absorption of visible light[3, 4]. Photo-excited electrons and holes can participate in redox reactions. Common applications as a photocatalyst include organic decomposition, water splitting for hydrogen production, and degradation of pollutants[5–8]. Oxygen vacancies and silver species help extend light absorption and improve catalytic performance. Mechanisms involve direct hole oxidation, hydroxyl radical formation, superoxide radical anions, and reactive oxygen species. The main advantages are visible light activity, chemical stability, tunable morphology, and moderate band positions. Drawbacks include fast recombination and low conversion efficiency. Overall, Ag_2WO_4 is a promising visible-light-driven catalyst for environmental and energy applications if the design is optimized to maximize charge separation and surface reactions[9].

MCRs refer to the multi-component that is an exceptionally and quick field that helps in forming complex structures from multi scaffolds in one pot reaction with high selectivity and economics. As a one-pot response, MCRs for the foremost portion bear the taken toll of great yields and are on a fundamental level not very the same as a two-component response in several perspectives 2 and permitted fast get to combinatorial libraries of natural particles for capable lead structure recognizable proof and progression in sedate discovery. Over the past decade, diverse advanced sequential MCRs have been made[10]. In the last two decades, a lot of researchers focused their work on an important class of heterocyclic polynuclear compounds called xanthenes and benzoxanthenamides. These classes have much importance in different fields, like pharmacological properties, as well as anti-antiviral, inflammatory, and antibacterial properties. In addition, xanthenes are also used as scaffolds in design dyes[11–14], in expansion to their employments as fluorescent substances in pH-sensitive for visualization of biomolecular gatherings[15], and laser innovations[16]. Related to this auxiliary lesson has been utilized as the flexible unit for the union of complex frameworks because of the chemical action of their inbuilt pyran ring[17]. Too, xanthenes's basic unit is displayed in a considerable number of standard items[18]. Subsequently, the blend of xanthene subordinates is of extraordinary significance and still has to be found unused engineered strategies uncommonly one-pot amalgamation that has a financial and natural impact.

Tuberculosis and the mycobacteria that cause it still cause the death of thousands of people around the world in spite of the presence of effective drugs. There was an assessed 1.2 million passing (2019) due to TB, and an extra 208,000 passings coming about from co-infection with HIV and TB[19]. The drug is currently used for tuberculosis (2018) with an effectiveness rate of up to 85%, but there are many side effects from it, including the period of treatment being too long. the long period of treatment increases bacterial resistance of bacteria which increases with the length of the treatment period, in addition to hepatic toxicity. Alarmingly, the advancement of multidrug-safe (MDR) and broadly drug-resistant (XDR) strains has undermined the ampleness of current anti-TB treatment: 57% of MDR cases were successfully treated around the world amid the 2017 cohort. Despite all the treatments offered, the problem of side effects and bacterial resistance to these treatments makes there a necessary and continuous need to innovate new, more advanced treatments and so we presented this new series of xanthenes as anti-mycobacterium tuberculosis.

Therefore, there is an urgent need for new antitubercular drugs, and it is necessary to find novel chemical scaffolds and mechanisms of action that can reduce treatment duration and prevent the emergence of drug resistance. Held on populaces of metabolically heterogeneous bacilli can frame within the granuloma microenvironments and survive treatment due to obtained phenotypic medicate resistance, indeed although numerous of the drugs as of now in clinical utilize are bactericidal[20]. A lot of the synthetic methods were prepared xanthenes in the literature[21, 22] unfortunately, most of these reactions can be carried out in the presence of macro-size protic acid, Lewis's acid, or another hazard catalyst, and most of these reactions were completed by reflux. The presented work suggested a new nano-size catalyst for the synthesis of xanthene derivatives.

EXPERIMENTAL

Materials

Silver nitrate ($AgNO_3$) and Sodium tungstate (Na_2WO_4) precursors were supplied by Sigma Aldrich Company and used without further purification. Commercial ethanol (75%) was used in the washing process.

Synthesis of Ag_2WO_4 Nano roads

In beaker A, one molar ratio of sodium tungstate 2.94 gm (Na_2WO_4: 293.82) was dissolved in 25 mL dist. water. In beaker B, a mixture of one molar ratio of one molar ratio of silver nitrate 1.69 gm ($AgNO_3$: 169.87) was added to 25 mL dist. water. The two mixtures were stirred separately at ambient room temperature for 10 minutes. The two aqueous solutions were transferred into Teflon-autoclave (TLA -100 mL) in a drying oven at 160 °C for 72 hours. After the appropriate time, the autoclave undergoes cooling at room temperature (25 °C). The final extraction precipitate underwent washing treatment with distilled water and ethanol to remove any soluble impurities or unreacted reagents and was dried in a normal oven at 60–80 °C for 3 hrs. The final pure product is collected as crystalline white fine powder Ag_2WO_4.

$$2AgNO_3 + Na_2WO_4 \rightarrow Ag_2WO_4 \downarrow + 2NaNO_3$$

Characterization of Ag_2WO_4 nano-roads and organic products

An X-ray diffraction system (model Bruker D8) was applied. A Vantech super speed position sensitive detector is equipped with it & a Gobel Mirror with a Cu K_α X-Ray tube. Measurements were taken from 4 to 80° in 2θ diffraction angle range. Morphological studies were visualized via scanning electron microscopy (SEM/JEOL JSM 6510 LV, USA).

Gallenkamp apparatus was used to measure the melting point of the end products. Nicolet iS10 was used in measure the FTIR. Jeol Resonance apparatus (Japan) at 125 MHz was used to measure the ^{13}C NMR. Jeol Resonance apparatus (Japan) at 500 MHz was used to measure the ^1H NMR. "$CDCl_3$ were used as NMR solvents". EuroVector instrument analyzer (EA3000 Series) was used to measure the molecular ion peaks and fragmentation of the organic end products.

Catalytic reaction procedure

10 mmol aldehyde, 10 mmol β-naphthol (10 mmol, 1.44 g), and 10 mmol dimedone (10 mmol, 1.4 g) were mixed. Then, 20 mol% Ag_2WO_4 was added and the obtained mixture was stirred at 60–70 °C. The progression yield for the targeted product was monitored by fluorescent silica based on aluminum sheets using UV lamp chromatography to monitor the reaction progress. Finally, the reaction mixture is poured into ethanol as a recrystallization solvent to purify the desired products. As a model example of spectroscopic data for the prepared molecules.

12-(3-(4-Bromophenyl)-1-phenyl-1H-pyrazol-4-yl)-9,9-dimethyl-8,9,10,12-tetrahydro-11H-benzo[a]xanthen-11-one (4i)

IR (anhydrous KBr): 1671 (C=O) , (1590 (C=C) cm^{-1}, ^1H-NMR (500 MHz, $CDCl_3$) δ ppm: 0.98 (s, $2CH_3$), 1.95 (s, CH_2), 2.10 (s, $2CH_2$), 5.67 (s, CH), 7.67–7.29 (m, 16 ArH + 1H-pyrazol); ^{13}C-NMR (125 MHz, $CDCl_3$) δ ppm: 190.85 (C=O), 149.11 (O-C=C), 148.50 (-C=N), 145.50–115.00 (24 Ar-C + 2 C in pyrazole ring), 49.05 (1C of $\underline{C}H_2CO$), 40.86 (1C of $\underline{C}H_2$), 31.75 (quaternary 1C), 29.85 (C of in pyran ring), 28.66 (2C of $2CH_3$) (Fig. 1). MS (EI) m/z = 574/576 [M^+, M^++2] $^+$, Anal. Calcd. For $C_{34}H_{27}BrN_2O_2$ (574.15): C, 70.96; H, 4.73; N, 4.87. Found: C, 70.91; H, 4.68; N, 4.77.

RESULTS AND DISCUSSION

Figure 2 reveals an SEM image of the synthesized silver tungstate. The image shows high-density nanorods of Ag_2WO_4 with smooth surfaces and uniform width. The nanorods have an elongated rod-like morphology with high aspect ratios, estimated to be around 10–20. The rods have widths of approximately 25–60 nm and they extend over several micrometers in length. The nanorods are reasonably straight along their major axis, showing some gentle bending or kinking. The rods appear separated from each other, with open spaces surrounding each nanostructure. There is no major aggregation observed. The ends of the nanorods are rounded and exhibit a club-like shape rather than being sharply tapered. The nanorod surfaces and edges look smooth without obvious defects, pits, or roughness. Overall, the SEM image demonstrates the successful synthesis of elongated Ag_2WO_4 nanorods with smooth surfaces, high aspect ratios, and no major aggregation. From the TEM images the roads formed are in the nano scale range.

The pattern shows a series of sharp, narrow diffraction peaks, indicating the crystalline nature of the synthesized material. Observable peaks can be indexed to the standard monoclinic phase reported by: (JCPDS Cardno. 12-0708) of Ag_2WO_4 with no secondary phases detected[23]. The strongest intensities are observed for the (121), (231), (002), (202), and (033) planes of Ag_2WO_4. The full width at half maxima (FWHM) of the peaks is relatively narrow, also confirming high crystallinity and few defects. The diffraction angles and d-spacings calculated from the pattern agree closely with literature

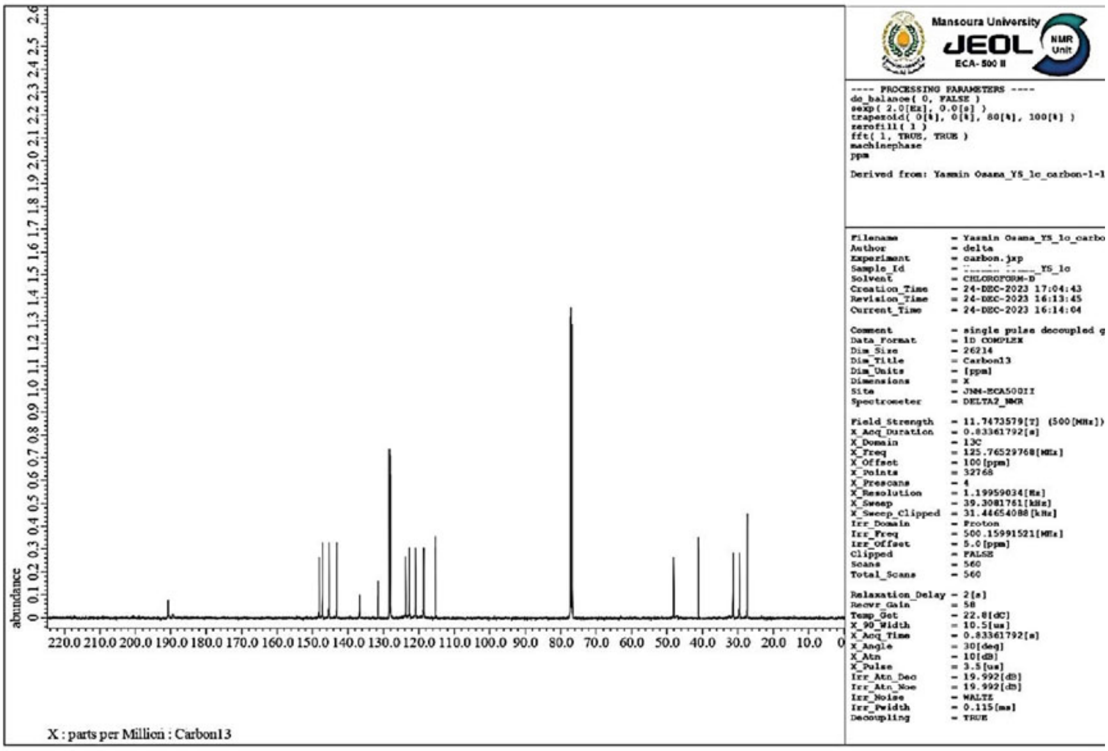

Figure 1. Carbon-NMR for the prepared 4i ligand

values. No impurity peaks related to unreacted precursors or side products are found (Fig. 3).

Subsequently, nano-catalysts have advanced some of the answers excellently in our collection research and continued modern synthetic method for heterocyclic compounds[24–34]. The presented work started with an optimization step to determine the best chemical condition and procedure for the targeted reaction. As explained in Scheme 1, a one-pot reaction is the best way for this reaction in which β-naphthol, aldehydes, and dimedone are mixed simultaneously until benzo-xanthenes are obtained.

The data obtained from the optimization step is summarized in Table 1 and the best condition of the presented reaction for the synthesis of benzo-xanthene derivatives can summarized as mixing the β-naphthol, aldehydes, and dimedone in 20% per mole of catalyst under solvent-free conditions at 60–70 ºC.

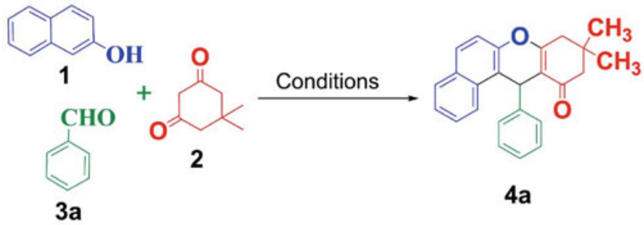

Scheme 1. Model example for optimization reaction between β-naphthol, benzaldehyde, and dimedone

Accidentally, during the reaction optimization by using different amounts of the targeted catalyst and various solvents, the prepared catalyst Ag_2WO_4 promoted the reaction in the acetonitrile solvent the reaction yielded

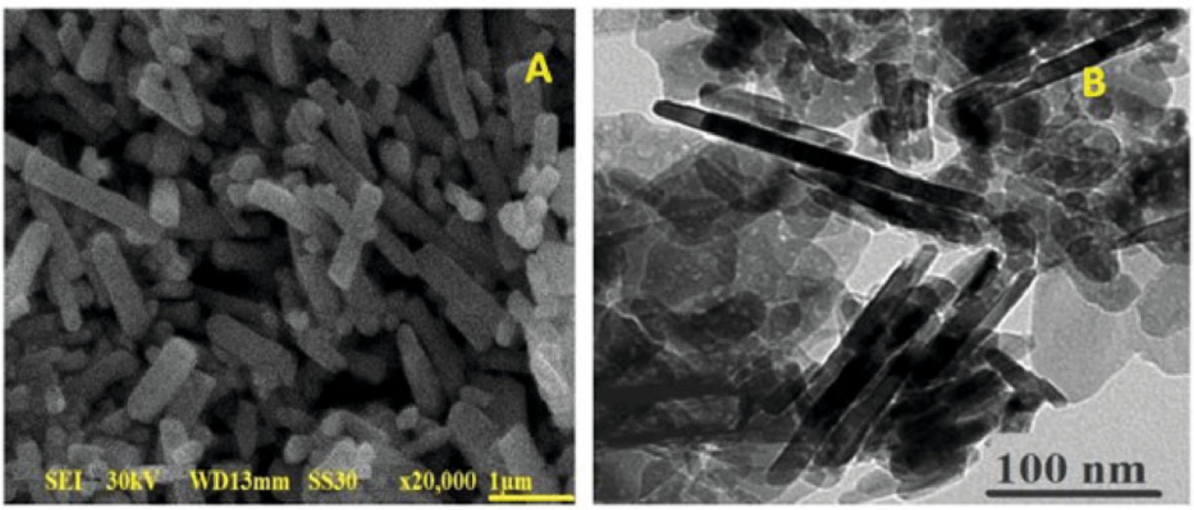

Figure 2. A is the SEM and B is the TEM images of the synthesized silver tungstate

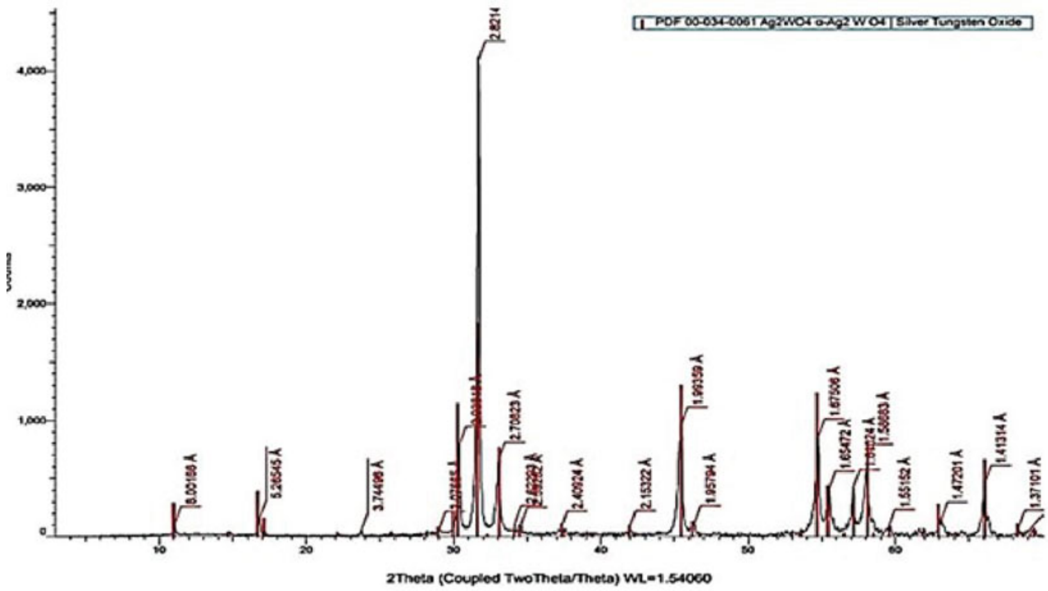

Figure 3. Reveals the XRD diffraction pattern of the synthesized silver tungstate

Table 1. Reaction optimization

Entry	Mole (%)	Catalyst	Solvent	Temp.	Time (min)	Yield (%)
1	20	Ag_2WO_4	Ethanol	reflux	60	60
2	20	Ag_2WO_4	CH_3CN	reflux	60	40 Mixed Products Scheme 2
3	20	Ag_2WO_4	$C_2H_4Cl_2$	reflux	60	79
4	10	Ag_2WO_4	Solvent-free	r.t.	60	80
5	15	Ag_2WO_4	Solvent-free	r.t.	60	82
7	20	Ag_2WO_4	Solvent-free	60–70 °C	60	91

less than 50% xanthene and the presence of a second product when monitoring by TLC. The two products separated and characterized as 4a by 40% yield and N-[(2-hydroxy-4,4-dimethyl-6-oxo-cyclohexenyl)-(phenyl) methyl]-acetamide (4'a) with m.p. 210 °C[35] by 20 % yield was separated as a byproduct, Which the acetonitrile solvent in product 4'a inter in the one pot reaction instead of β-naphthol Scheme 2.

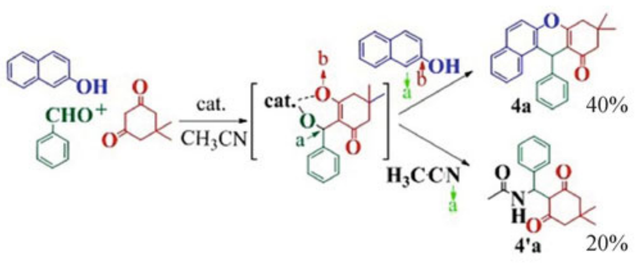

Scheme 2. Reaction between β-naphthol, benzaldehyde, and dimedone in acetonitrile

After the optimization step, the reaction was progressed by changing the aldehyde with a variety of substitutions to approve the efficiency of the presented procedure the data obtained is summarized in Table 2.

A plausible mechanism explains the main role of the catalyst through increasing the polarization power of the carbonyl group in aldehydic compounds and this increases the nucleophilic attack reaction from β-naphthol Scheme 3. Finally, the obtained enones were added to the enolic form of dimedone and after the dehydration step, the final benzoxanthenes were obtained.

Molecular docking studies

The presented data was designed and calculated using MOE 2014.0901 software. The synthesized xanthene derivatives and xanthene-9-carboxylic acid were validated as mycobacterium tuberculosis ArgC inhibitors. The most common calculation used in the detection of ligand affinity is energy score values the lower value explaining

Table 2. Synthesis of different tetrahydrobenzo[a]xanthene-11-one deivatives at 60–70 °C under solvent free condition

Entry	Aldehyde	Products	Time (min)	Yield %
1	Benzaldehyde	4a	60	91*
2	Toluene	4b	90	88*
3	*p*-Anisaldehyde	4c	90	82*
4	Piperonal	4d	80	83*
5	Vanillin	4e	60	90*
6	*p*-(F)-Benzaldehyde	4f	30	96*
7	*m*-(Cl)-Benzaldehyde	4g	30	95*
8	*p*-(Cl)-Benzaldehyde	4h	40	93*
9	3-(4-Bromophenyl)-1-phenyl-1*H*-pyrazole-4-carbaldehyde	4i	40	77
*Melting points of cpds matches with literature values[21, 22].				

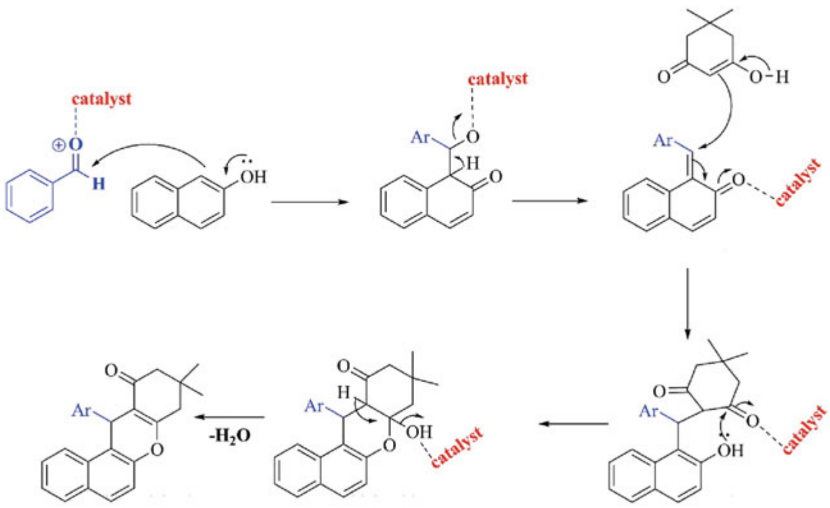

Scheme 3. The suggested mechanism

that the drug is more potent for the active site in the targeted enzyme. The data obtained refers to all the nine prepared compounds having lower E score values in kcal/mol. Then the literature reference[36] explains that the prepared compound can be a good mycobacterium tuberculosis ArgC inhibitor (Fig. 4).

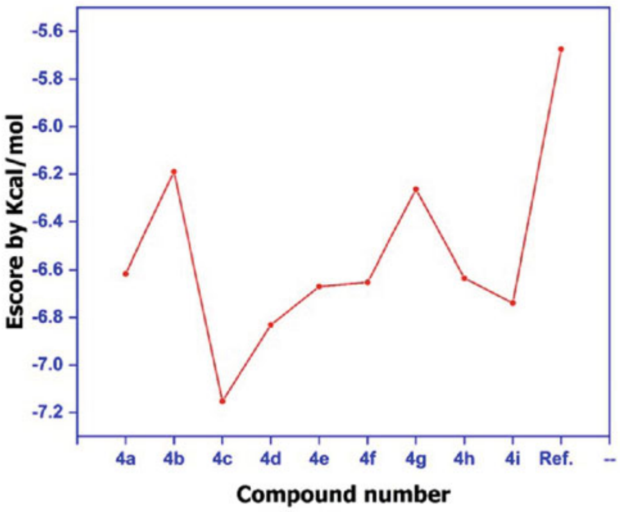

Figure 4. The energy score validation of the prepared ligands 4a–4i and reference molecule in (red color point)

The interaction between the prepared ligands and the active side amino acid residues demonstrated a binding process and pharmacodynamics phase for the prepared ligands compared with the literature references. Generally, it forms more than two electrostatic bonds. Figure 5 presents the 2D ligand-receptor interaction of compound 4e the binding process is fixed by four electrostatic bonds compared with the reference molecule. Also, the 3D gives a clearer structure explaining the ligand active site complex (Fig. 6).

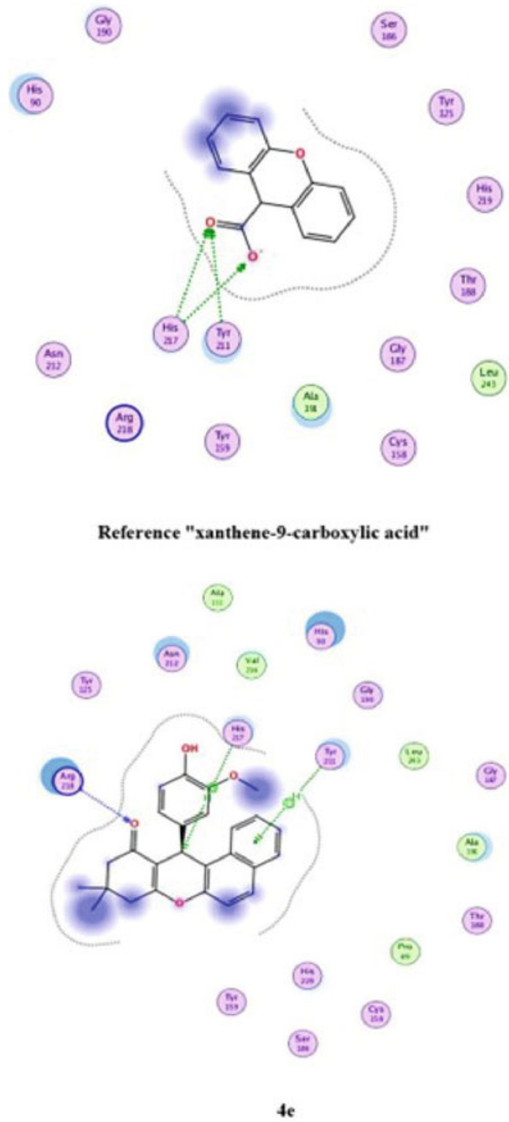

Figure 5. ligand 4e and reference molecule interaction with a targeted receptor "tuberculosis ArgC" in 2D structure

CONCLUSION

Ag_2WO_4 nanorods were successfully synthesized using a simple and green hydrothermal chemical method. Characterization for the precipitate by XRD and SEM confirmed the formation of crystalline monoclinic Ag_2WO_4 nanorods with smooth surfaces and high aspect ratios. The Ag_2WO_4 nanorods were applied as an efficient catalyst for the one-pot synthesis of tetrahydrobenzo[a]xanthene-11-one derivatives via the three-component reaction of β-naphthol, dimedone, and various aldehydes. The solvent-free reaction at 60–70 °C with 20 mol% Ag_2WO_4 gave yields up to 96%. Molecular docking studies were performed to evaluate the binding affinity of the synthe-

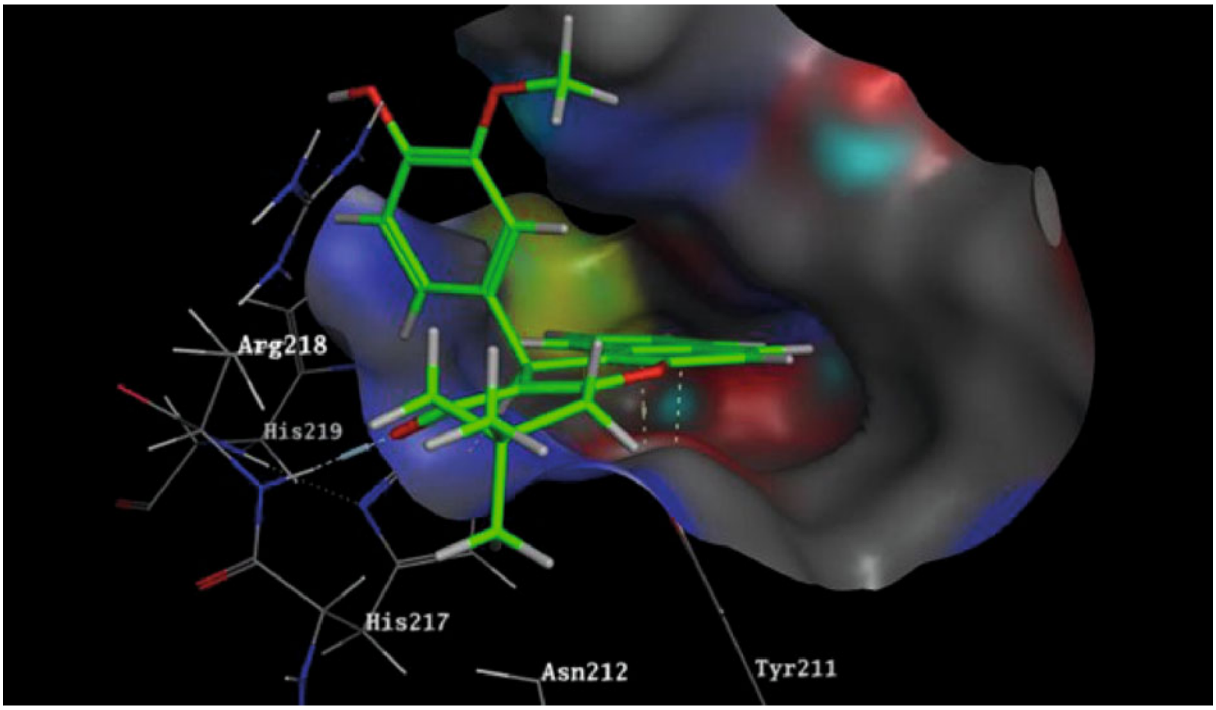

Figure 6. Ligand 4e interaction with targeted receptor "tuberculosis ArgC" in 3D structure

sized xanthene compounds against the Mycobacterium tuberculosis enzyme ArgC. The docking results showed stronger binding affinity and lower energy scores compared to the reference ligand xanthene-9-carboxylic acid, suggesting good potential as an anti-TB inhibitor. The Ag_2WO_4 nanorod catalyst enabled an efficient one-pot synthesis of xanthene derivatives, which were validated by docking as promising anti-TB drug candidates against the ArgC enzyme target.

FUNDING

This research was funded by King Saud University, Riyadh, Saudi Arabia through Researchers Supporting Project No. (RSP2024R359).

ACKNOWLEDGMENTS

Authors are grateful to King Saud University, Riyadh, Saudi Arabia for funding the work through Researchers Supporting Project No. (RSP2024R359).

CONFLICT OF INTEREST

The authors declare that they have no competing interests.

LITERATURE CITED

1. Araujo, R.O., Santos, V.O., Ribeiro, F.C., Chaar, J.D.S., Falcão, N.P. & de Souza, L.K. (2021). One-step synthesis of a heterogeneous catalyst by the hydrothermal carbonization of acai seed. *Reac. Kinet. Mech. Cat.* 134, 199–220. DOI: 10.1007/s11144-021-02059-9.

2. Yan, H., Ren, Y., Zhang, R., Chang, F., Wei, Q. & Xu, J. (2023). A One-Pot Hydrothermal Preparation of High Loading Ni/La_2O_3 Catalyst for Efficient Hydrogenation of Cinnamaldehyde. *Catalysts* 13(2), 298. DOI: 10.3390/catal13020298.

3. Wang, X., Fu, C., Wang, P., Yu, H. & Yu, J. (2013). Hierarchically porous metastable β-Ag_2WO_4 hollow nanospheres: controlled synthesis and high photocatalytic activity. *Nanotechnology* 24, 165602. DOI: 10.1088/0957-4484/24/16/165602.

4. Roca, R.A., Lemos, P.S., Gracia, L., Andrés, J. & Longo, E. (2017). Uncovering the metastable γ-Ag_2WO_4 phase: a joint experimental and theoretical study. *RSC Adv.* 7, 5610–5620. DOI: 10.1039/C6RA24692C.

5. Wu, G., Liu, Q., Wang, J., Cai, Z., Li, H., Zhang, T., Lu, R., Li, P., Han, J. & Xing, W. (2021). Synthesis of silver-based composite photocatalysis material and its visible-light-driven photocatalytic degradation of dye pollutants. *Fresenius Environ. Bull.* 30, 9696–9706.

6. Al-Wasidi, A.S. & Abdelrahman, E.A. (2023). Significant photocatalytic decomposition of malachite green dye in aqueous solutions utilizing facilely synthesized barium titanate nanoparticles. *Discover Nano.* 18, 97. DOI: 10.1186/s11671-023-03873-x.

7. Al-Wasidi, A.S., Naglah, A.M., Saad, F.A. & Abdelrahman, E.A. (2022). Modification of silica nanoparticles with 1-hydroxy-2-acetonaphthone as a novel composite for the efficient removal of Ni(II), Cu(II), Zn(II), and Hg(II) ions from aqueous media. *Arab. J. Chem.* 15, 104010. DOI: 10.1016/j.arabjc.2022.104010.

8. Al-Wasidi, A.S., Saad, F.A., Munshi, A.M. & Abdelrahman, E.A. (2023). Facile synthesis and characterization of magnesium and manganese mixed oxides for the efficient removal of tartrazine dye from aqueous media. *RSC Adv.* 13, 5656–5666. DOI: 10.1039/D3RA00143A.

9. Assis, M.D., Castro, M.S., Aldao, C.M., Buono, C., Ortega, P.P., Teodoro, M.D., Andres, J., Gouveia, A.F., Simões, A.Z., Longo, E. & Macchi, C.E. (2023). Disclosing the nature of vacancy defects in α-Ag2WO4. *Mater. Res. Bull.* 164, 112252. DOI: 10.1016/j.materresbull.2023.112252.

10. Jia, X., Xu, G., Du, Z. & Fu, Y. (2018). Cu(BTC)-MOF catalyzed multicomponent reaction to construct 1,4-disubstituted-1,2,3-triazoles. *Polyhedron* 151, 515–519. DOI: 10.1016/j.poly.2018.05.058.

11. Zelefack, F., Guilet, D., Fabre, N., Bayet, C., Chevalley, S., Ngouela, S., Lenta, B.N., Valentin, A., Tsamo, E. & Dijoux-Franca, M.G. (2009). Cytotoxic and antiplasmodial xanthones from Pentadesma butyracea. *J. Nat. Prod.* 72, 954–957. DOI: 10.1021/np8005953.

12. Manathanath, M., Sasidharan, S., Saudagar, P., Panicker, U.G. & Sujatha, S. (2022). Photodynamic evaluation of triazine appended porphyrins as anti-leishmanial and anti-tumor agents. *Polyhedron* 217, 115711. DOI: 10.1016/j.poly.2022.115711.

13. Evangelinou, O., Hatzidimitriou, A.G., Velali, E., Pantazaki, A.A., Voulgarakis, N. & Aslanidis, P. (2014). Mixed-ligand copper (I) halide complexes bearing 4, 5-bis (diphenylphosphano)-9, 9-dimethyl-xanthene and N-methylbenzothiazole-2-thione: Synthesis, structures, luminescence and antibacterial activity mediated by DNA and membrane damage. *Polyhedron* 72, 122–129. DOI: 10.1016/j.poly.2014.02.002.

14. Zolfigol, M.A., Moosavi-Zare, A.R., Arghavani-Hadi, P., Zare, A., Khakyzadeh, V. & Darvishi, G. (2012). WCl6 as an efficient, heterogeneous and reusable catalyst for the preparation of 14-aryl-14 H-dibenzo[a, j]xanthenes with high TOF. *RSC Adv.* 2, 3618–3620. DOI: 10.1039/C2RA00014H.

15. Liu, J., Diwu, Z. & Leung, W.Y. (2001). Synthesis and photophysical properties of new fluorinated benzo[*c*]xanthene dyes as intracellular pH indicators. *Bioorg. Med. Chem. Lett.* 11, 2903–2905. DOI: 10.1016/S0960-894X(01)00595-9.

16. Ahmad, M., King, T.A., Ko, D.K., Cha, B.H. & Lee, J. (2002). Performance and photostability of xanthene and pyrromethene laser dyes in sol-gel phases. *J. Phys. D: Appl. Phys.* 35, 1473. DOI: 10.1088/0022-3727/35/13/303.

17. Adjadi, S., Akbari, M., Kahangi, F.G. & Heravi, M.M. (2020). Acidic polymer containing sulfunic acid and carboxylic acid groups heterogenized with natural clay: A novel metal free and heterogeneous catalyst for acid-catalyzed reactions. *Polyhedron* 179, 114375. DOI: 10.1016/j.poly.2020.114375.

18. Chen, X., Pradhan, T., Wang, F., Kim, J.S. & Yoon, J. (2012). Fluorescent chemosensors based on spiroring-opening of xanthenes and related derivatives. *Chem. Rev.* 112, 1910–1956. DOI: 10.1021/cr200201z.

19. World Health Organization, Geneva, 2019. Global tuberculosis report 2019. (https://www.who.int/publications/i/item/9789241565714) (accessed 1 March 2024).

20. Vilcheze, C. & Jr, W.R.J. (2019). The Isoniazid Paradigm of Killing, Resistance, and Persistence in *Mycobacterium tuberculosis*. *J. Mol. Biol.* 431, 3450–3461. DOI: 10.1016/j.jmb.2019.02.016.

21. Kai, G., Hualan, W., Shuxin, W., Ying, W. & Jinghua, C. (2015). Efficient synthesis of 1,8-dioxo-octahydroxanthenes catalyzed by β-cyclodextrin grafted with butyl sulfonic acid in aqueous media. *Chin. J. Catal.* 36, 1249–1255. DOI: 10.1016/S1872-2067(15)60888-9.

22. Li, J., Lu, L. & Su, W. (2010). A new strategy for the synthesis of benzoxanthenes catalyzed by proline triflate in water. *Tetrahedron Lett.* 51, 2434–2437. DOI: 10.1016/j.tetlet.2010.02.149.

23. George, T., Joseph, S. & Mathew, S. (2005). Synthesis and characterization of nanophased silver tungstate. *Pramana* 65, 793–799. DOI: 10.1007/BF02704077.

24. G.E. Said, M. Tarek, A.A. Zen, A.A. Almehizia, A.M. Naglah, T.K. Khatab, Novel Cobalt/vitamin B^3 metal-organic framework as nano-catalyst in synthesis of some new bis-indole derivatives with staking validation towards Salmonella DNA. *J. Organometallic Chemistry* 1008 (2024) 123074. DOI: 10.1016/j.jorganchem.2024.123074.

25. Abdel-Latif, E., Khatab, T.K., Fekri, A. & Khalifa, M.E. (2021). Synthesis of New Binary Thiazole-Based Heterocycles and Their Molecular Docking Study as COVID-19 Main Protease (Mpro) Inhibitors. *Russ. J. Gen. Chem.* 91, 1767–1773. DOI: 10.1134/S1070363221090231.

26. Shaker, N., Kandil, E.M., Osama, Y., Khatab, T.K. & Khalifa, M.E. (2021). ZnCl2/SiO2 as a New Catalyst for the Eco-Friendly Synthesis of N-Thiocarbamoyl Pyrazoles and Thiosemicarbazones with Antioxidant and Molecular Docking Evaluation as (UppS) Inhibitor. *Curr. Org. Chem.* 25, 2037–2044. DOI: 10.2174/1385272825666210809142341.

27. Khatab, T.K., Kandil, E.M., Elsefy, D.E. & El-Mekabaty, A. (2021). A One-Pot Multicomponent Catalytic Synthesis of New 1H-Pyrazole-1-Carbothioamide Derivatives with Molecular Docking Studies as COX-2 Inhibitors. *Biointerf. Res. Appl. Chem.* 11, 13779–13789. DOI: 10.33263/BRIAC116.1377913789.

28. Khatab, T.K., Mubarak, A.Y. & Soliman, H.A. (2017). Design and Synthesis Pairing Between Xanthene and Tetrazole in Pentacyclic System Using Tetrachlorosilane with Aurora Kinase Inhibitor Validation. *J. Heter. Chem.* 54, 2463–2470. DOI: 10.1002/jhet.2846.

29. Khatab, T.K. Hassan, A.S. & Hafez, T.S. (2019). V2O5/SiO2 as an efficient catalyst in the synthesis of 5-amino-pyrazole derivatives under solvent free condition. *Bull. Chem. Soc. Ethiop.* 33, 135–142. DOI: 10.4314/bcse.v33i1.13.

30. Soliman, H.A. & Khatab, T.K. (2018). New Approach for Tetrachlorosilane Promoted One-Pot, Condensation Reaction for Tetrahydrobenzo[a]Xanthene-11-Ones with Docking Validation as Aurora Kinase Inhibitor. *Silicon* 10, 229–233. DOI: 10.1007/s12633-016-9421-0.

31. Soliman, H.A., Khatab, T.K. & Abdel-Megeid, F.M. (2016). Utilization of bromine azide to access vicinal-azidobromides from arylidene malononitrile. *Chin. Chem. Lett.* 27, 1515–1518. DOI: 10.1016/j.cclet.2016.03.026.

32. Said, G.E., Tarek, M., Al-Wasidi, A.S., Naglah, A.M., Almehizia, A.A. & Khatab, T.K. (2024). Niacin based MOF as efficient nano-catalyst in the synthesis of some new benzothiazoles and benzimidazoles as anti-Alzheimer (AChE inhibitors). *J. Mol. Struct.* 1311, 138462. DOI: 10.1016/j.molstruc.2024.138462.

33. Almehizia, A.A., Naglah, A.M., Zen, A.A., Khatab, T.K. & Hassan, A.S. (2024). TCS/ZnCl2 as a controlled reagent for the Michael addition and heterocyclic cyclization based on the phenyl pyrazolone scaffold with docking validation as a Covid-19 protease inhibitor. *Bull. Chem. Soc. Ethiop.* 38, 1119–1127. DOI: 10.4314/bcse.v38i4.24.

34. Hassan, A.S., Hafez, T.S., Ali, M.M. & Khatab, T.K. (2016). Design, synthesis and cytotoxic activity of some new pyrazolines bearing benzofuran and pyrazole moieties. *Res. J. Pharm. Biol. Chem. Sci*. 7, 417–429. DOI: http://www.rjpbcs.com/pdf/2016_7(4)/[60].pdf

35. Javid, A., Heravi, M.M. & Bamoharram, F.F. (2012). One-pot three-component synthesis of β-acetamido carbonyl compounds catalyzed by heteropoly acids. *Monatsh. Chem.* 143, 831–834. DOI: 10.1007/s00706-011-0669-1.

36. Gupta, P., Thomas, S.E., Zaidan, S.A., Pasillas, M.A., Cory-Wright, J., Sebastián-Pérez, V., Burgess, A., Cattermole, E., Meghir, C., Abell, C. & Coyne, A.G. (2021). A fragment-based approach to assess the ligandability of ArgB, ArgC, ArgD and ArgF in the L-arginine biosynthetic pathway of *Mycobacterium tuberculosis*. *Comput Struct Biotechnol J.* 19, 3491–3506. DOI: 10.1016/j.csbj.2021.06.006.